Cleaner Engineering and Technology 23 (2024) 100823

Contents lists available at ScienceDirect

Cleaner Engineering and Technology

journal homepage: www.sciencedirect.com/journal/cleaner-engineering-and-technology

Transforming waste into valuable resources: Recycled nitrile-butadiene rubber scraps filled with electric arc furnace slag

Anna Gobetti [a,*], Giovanna Cornacchia [b], Giorgio Ramorino [a]

[a] Materials Science and Technology at Department of Mechanical and Industrial Engineering, University of Brescia, Via Branze 38, 25123, Brescia, Italy
[b] Metallurgy at Department of Mechanical and Industrial Engineering, University of Brescia, Via Branze 38, 25123, Brescia, Italy

ARTICLE INFO

Keywords:
EAF slag reuse
Slag characterization
Vulcanized rubber recycling
Rubber/slag composites
Waste valorization through industrial symbiosis

ABSTRACT

This study investigates the valorization of two industrial waste streams - nitrile butadiene rubber (NBR) scraps and electric arc furnace (EAF) slag – in the development of recycled NBR compounds filled with EAF slag as filler. A new recycling method for NBR scraps is employed via calendering at room temperature without the need for curatives, chemical agents, or pre-grinding. The resulting recycled NBR is then used as a matrix for EAF slag particles to produce sustainable rubber compounds that are entirely recycled. Characterization reveals that incorporating EAF slag enhances the devulcanization process of recycled NBR during recycling. The filler grain size affects composite properties like hardness, crosslink density, and tensile modulus, with finer slag particles (<50 μm) exhibiting improved reinforcement due to increased interaction surface with the rubber matrix. Dynamic mechanical analysis indicates that recycled NBR filled with EAF slag exhibits a more significant Payne effect compared to unfilled recycled NBR, due to filler-matrix interactions. Interestingly, EAF slag facilitates the rapid fractional recovery of the low-strain storage modulus after experiencing high-amplitude strain, ascribed to the formation of a rigid rubber layer around the slag particles.

Overall, the findings highlight the potential to valorize these two waste materials effectively by producing functional recycled NBR/EAF slag composites with desirable properties through a simple, industrially viable recycling method without capital-intensive equipment. This represents both environmental and economic benefits through waste valorization and industrial symbiosis.

1. Introduction

The recycling and reuse of industrial waste materials are of increasing importance from both environmental and economic perspectives (Gobetti et al., 2024a, 2024b). Preserving resources and recycling materials is essential for securing the sustainable utilization of natural reserves, ensuring their availability for future generations, and mitigating environmental footprints (Hummen and Sudheshwar, 2023; Gobetti and Ramorino, 2020).

To achieve these goals, numerous research efforts have focused on finding innovative ways to transform waste into valuable resources. This circular economy approach gains even greater significance when the valorization of one waste material is achieved by exploiting the unique characteristics of another waste stream, exemplifying the principles of industrial symbiosis. The present research is concerned with two significant waste streams: the issue of recycling crosslinked elastomers and the exploration of innovative applications for steelmaking waste, namely steel slag.

Recycling and reprocessing vulcanized elastomers like rubber compounds present significant challenges due to their covalently crosslinked network structure. After the vulcanization process, the material becomes insoluble and cannot melt due to its crosslinked network, unlike thermoplastic polymers which can be readily melted and reshaped during recycling through the application of heat (Gobetti and Ramorino, 2020; Grause et al., 2011).

Rubber is a versatile polymer broadly used in products such as tires, seals, hoses, belts, and many others due to its unique viscoelastic properties. However, its production process poses significant environmental challenges, as it generates a substantial amount of industrial scrap material. These scraps derive not only from defective parts but are also inherent to the production process. In many cases, the rubber molding process requires subsequent deflashing to remove excess flash, as well as the removal of sprue and runner systems from the mold. The quantity of scrap produced can be around 20–30% of the total material

* Corresponding author.
E-mail addresses: anna.gobetti@unibs.it (A. Gobetti), giovanna.cornacchia@unibs.it (G. Cornacchia), giorgio.ramorino@unibs.it (G. Ramorino).

https://doi.org/10.1016/j.clet.2024.100823
Received 1 July 2024; Received in revised form 7 October 2024; Accepted 13 October 2024
Available online 18 October 2024

processed. This significant amount of waste underscores the need for effective recycling methods to reduce material waste from rubber manufacturing operations. Unlike thermoplastic scrap, vulcanized rubber scrap cannot be directly reintroduced into the production cycle due to its crosslinked network structure, which is a result of the vulcanization process. Consequently, recycling vulcanized elastomeric scrap requires more complex processes, such as devulcanization or selective breakdown of crosslinks to reprocess the material (Chittella et al., 2021).

The reuse and reclamation of rubber waste, encompassing both industrial and post-consumer scraps, have become pivotal aspects of waste management strategies, particularly within industrial contexts (Chittella et al., 2021). Conventional methods for the disposal of rubber waste often involve practices such as open dumping, landfilling, incineration, or pulverization into fine particles, with only a small fraction being subjected to recycling or reuse (Chittella et al., 2021; Leong et al., 2023; Liu et al., 2020). The successful recycling of crosslinked elastomers, such as vulcanized rubber, necessitates the cleavage of crosslinks without causing detrimental effects to the polymer chains (Adhikari et al., 2019). Various methods have been explored for managing rubber waste, encompassing thermal, mechanical, physical, chemical, and biological approaches, each with its own set of parameters and chemicals to facilitate devulcanization while minimizing degradation (Chittella et al., 2021). In the domain of mechanical recycling, numerous studies have investigated devulcanization techniques employing different additives and methodologies to enhance mechanical properties (Rooj et al., 2011; Sabzekar et al., 2016; de Sousa et al., 2020).

On the other side, the EU steelmaking industry produced about 60 Mton of crude steel, of which 43,3% was derived from EAF (EUROFER The European Steel association, 2023). Widening the perspective globally, it is estimated that steel production from EAF, i.e. from scrap in a circular context, currently around 30%, will reach 53% by 2050 (The 15th Global Slag Conference, 2023). The steelmaking process using EAF inevitably involves the production of black slag, which plays a pivotal role in eliminating impurities from the molten steel. Alongside its primary function of absorbing deoxidation products and impurities from the molten steel (Teo et al., 2014), slag production is unavoidable due to the critical functions it performs in the production of high-quality steel. However, given the large quantities produced (about 10–15% of the steel produced), it is a by-product that must be recovered. This recovery will become increasingly important from the perspective of a circular steel economy that promotes the use of ferrous scrap as raw material in the electric furnace process. EAF slag is widely used in the construction industry as an artificial aggregate (Manso et al., 2004; Netinger Grubeša et al., 2016; Aliyah et al., 2023) due to its chemical-physical similarities to volcanic rock (Pisciotta, 2020). However, it is estimated that a significant quantity is still disposed of in landfills. Therefore, exploring new applications to further reduce landfill disposal is mandatory. In recent years, the use of slag as a sustainable filler for different polymers has been studied, with emphasis on rubber compounds showing promising results (Gobetti et al., 2021a, 2021b, 2022, 2023a, 2023b, 2023c, 2024b, 2024c). Incorporating EAF slag into polymer matrices like polypropylene, epoxy resin, nitrile-butadiene rubber (NBR), and recycled rubber tires enhances the composites' stiffness, albeit with a reduction in toughness (Gobetti et al., 2021a, 2022). The addition of slag as filler affects both static and dynamic behavior of nitrile-butadiene rubber compounds, increasing their energy storage and dissipation capabilities (Gobetti et al., 2023b). Furthermore, slag can be a valuable substitute for natural sand in epoxy resin (Gobetti et al., 2021b), calcium carbonate (Gobetti et al., 2023a, 2024c), and even a partial replacement for carbon black in NBR (Gobetti et al., 2024c). Additionally, composites of geopolymeric steel slag particles exhibit low moisture absorption and potential for sustainable applications such as ballistic vests, highlighting the feasibility of reusing waste materials for environmental benefits (Santos et al., 2020).

The present study simultaneously addresses the issue of recycling two distinct industrial wastes: rubber scrap and EAF slags. The rubber waste considered in this study is NBR industrial scrap generated during product manufacturing. NBR is a specialized synthetic rubber copolymer known for its excellent resistance to oil, fuel, and heat. It is widely used in automotive seals and roll coverings, as well as in the oil and gas industries.

The NBR scrap is recycled via a calendering process, without the addition of any curatives or chemical agents, neither heat. Furthermore, no pre-treatment of the waste is required to obtain granules or chips. This mechanical devulcanization approach significantly differs from conventional thermal-mechanical or mechano-chemical recycling methods, which typically involve specialized equipment, elevated temperatures, devulcanizing additives, and grinding pre-treatments (Dorigato et al., 2023). The proposed calendering technique relies solely on the shear forces imparted during the calendering operation to make the vulcanized rubber re-formable in a new shape. Notably, this method does not require any specialized recycling machinery, as it utilizes standard calenders commonly available in rubber processing facilities. This enables manufacturers to valorize their own scrap material without significant capital investment. Moreover, the avoidance of rubber scrap grinding is a remarkable aspect concerning recent regulations (EU regulation 2023/2055 (European Commission, 2023)) on microplastics. These regulations have notably impacted the application of end-of-life rubber tire granules, particularly their use as infills for football fields. This study aims to investigate a novel approach for recycling NBR scrap and subsequently use the resulting recycled NBR as a matrix for EAF slag particles to produce functional composites. Initially, the EAF slag was analyzed for its particle size distribution, chemical composition, and mineralogical phases. The leaching characteristics of various slag grain size ranges were also studied. This included investigating the effect of EAF slag (10% v/v) as a filler, and assessing different granulometric ranges (0–50 μm and 50–100 μm) with the same filler volume fraction. The effects of EAF slag filler content and particle size on the crosslink density were evaluated using Flory-Rehner equation (Flory et al., 1943). Additionally, the mechanical properties and dynamic viscoelastic behavior of the recycled NBR compounds were thoroughly characterized and discussed using the Kraus and Ulmer prediction models (Ulmer, 1996; Kraus, 1984).

Based on the achieved results, it is evident that both industrial wastes, have significant potential for exploitation. This not only offers environmental benefits by reducing waste disposal but also provides economic advantages.

2. Materials and methods

2.1. Materials

The studied EAF slag originates from an Italian steel plant and is obtained by a method involving rapid cooling with high-pressure cold air, resulting in the formation of spherical slag particles (Gao et al., 2021).

The slag was then utilized as a filler after being ground with a blade granulator at 500 rpm for about 10 min, starting from an initial grain size lower than 1 cm to achieve a suitable grain size for the intended application. The slag was subsequently sieved into four different grain size ranges: 0–50 μm, 50–100 μm, 100–150 μm, and 150–300 μm in order to evaluate the granulometric distribution at the end of the used grinding process.

For the present study, two particle size ranges (0–50 μm and 50–100 μm) were selected, as particle sizes above 100 μm characterise a filler that is highly degradative to the mechanical properties of elastomeric compounds (Leblanc, 2002).

The recycled industrial NBR scrap, employed as the base material, is a commercial NBR sourced from Novotema Spa in Villongo BG, Italy. The composition is provided in Table 1.

The industrial rubber scrap was recycled through a calendering process, using industrial scraps generated by injection molding at a

Table 1
Composition of characterized NBR.

Ingredient	phr
NBR	100
Carbon black	40
Plasticizers	15
ZnO	5
Stearic acid	1
Sulfur	1

temperature of 170 °C. The calendering machine utilized in this process was supplied by Gaoge-tech instrument. Throughout the calendering procedure, the rubber undergoes multiple stages where the temperature rises to 80 °C caused by the shear stresses generated by the rotating cylinder, initiating softening and plasticization of the material. This results in a sheet with a thickness of approximately 2–3 mm upon completion of the calendering process, during which fillers can be compounded with the rubber matrix. The recycling and compounding process is illustrated in Fig. 1a. It is important to note that in the context of this study, the term "room temperature" refers to a recycling process that does not involve an external heat source. However, the high frictional stresses generated during the process result in temperatures that are comparable to those typically used to reduce the viscosity of the raw compound in the injection molding process, without initiating vulcanization.

The material was then compression molded at 40 MPa and 180 °C for 15 min to produce test plates. Specimens were mechanically punched out from these plates (see Fig. 1b).

For comparison, a virgin NBR was also tested as reference commercial compound. To summarize, the analyzed materials include:

- Virgin NBR
- Recycled NBR
- Recycled NBR containing 10% [v/v] EAF slag 0–50 μm
- Recycled NBR containing 10% [v/v] EAF slag 50–100 μm

The selection of 10% by volume EAF slag was determined by preliminary tests which demonstrated that this quantity represents the maximum feasible filler content for efficient compounding and recycling processes. Concentrations above 10% result in complications that render the process less implementable in an industrial setting.

2.2. Methods

2.2.1. EAF slag characterization

The grain size distribution of the EAF slag was determined using a series of stacked sieves with progressively finer mesh sizes (500, 300, 150, 100, 50 μm). The filler sample was passed through the stacked sieve tower, and particles were retained in different sieves based on size, allowing for quantification of the size distribution.

The chemical composition of the EAF slag was analyzed by XRF.

The mineral phases present in the EAF slag were identified by SEM combined with EDXS. The slag sample was prepared by standard metallographic polishing methods and sputtered with gold before analysis.

Leaching tests were performed according to CEN EN 12457-2 standard (CEN EN 12457-2, 2002) on EAF slag with a grain size lower than 4 mm. Additionally, size-fractionated samples were tested: 0–50 μm, 50–100 μm, 100–150 μm, 150–300 μm. A liquid-to-solid ratio of 10:1 and a mixing time of 24 h were used. Metal concentrations (Cr, Mo, V) in the eluates were measured by ICP-OES using an Avio 200 PerkinElmer spectrometer (Milano, Italy).

2.2.2. Compounds characterization

The crosslink density was assessed through a swelling test. Approximately 400 mg samples were cut and submerged in toluene for 48 h at room temperature. Afterward, the samples were dried in an oven equipped with a suction system at 80 °C for 24 h before being weighed. The degree of equilibrium swelling is affected by the crosslink density as well as the attractive interactions between the solvent and the polymer. Theoretical swelling levels are predicted using the Flory–Rehner equation. (Equation (1)) (Flory et al., 1943; Mok and Eng, 2018; Valentín et al., 2008):

$$\nu = -\frac{\ln(1 - v_{Rf}) + v_{Rf} + \chi v_{Rf}^2}{V_s\left(v_{Rf}^{1/3} - \frac{2v_{Rf}}{f}\right)} \quad \text{Equation 1}$$

Where:

ν Is the crosslink density [mol/cm^3].

Vs = 106.52 (m^3/mol) is the toluene molar volume;

f = 4 for tetra functional network junctions;

χ Is the Flory–Huggins solvent–polymer interaction parameter determined according to Equation (2);

v_{Rf} is the volume fraction of elastomer in the swollen mass, deter-

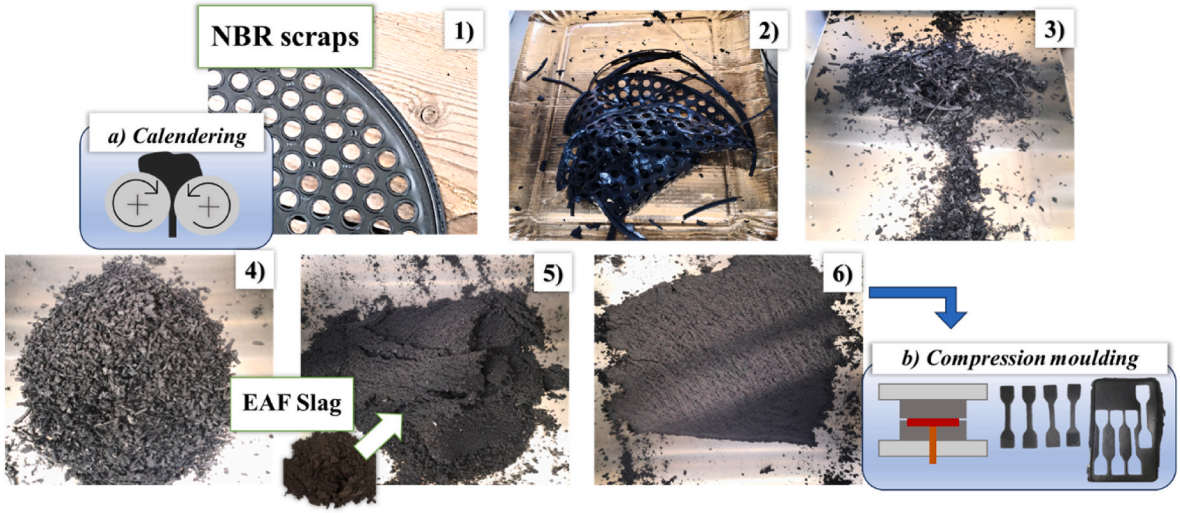

Fig. 1. Production process of recycled NBR compound filled with EAF slag via a) calendering process in several steps (figures from 1 to 6), followed by b) Compression molding process.

mined according to Equation (3).

The Flory–Huggins solvent–polymer interaction parameter is 0.42, determined using the Bristow and Watson semi-empirical equation (Barikani and Hepburn, 1992; Bristow and Watson, 1958a, 1958b):

$$\chi = \beta_1 + \frac{V_S}{RT}(\delta_2 - \delta_1)^2 \quad \text{Equation 2}$$

Where:

β_1 is the lattice constant approximately 0,34 (Barikani and Hepburn, 1992; Bernal-Ortega et al., 2023);

$\delta_1 = 19.57\ (MPa)^{1/2}$ is the solubility parameter of NBR (33% acrylonitrile content) (Liu et al., 2022), $\delta_2 = 18.2\ (MPa)^{1/2}$ is the solubility parameter of toluene (Yehia and El-Sabbagh, 2007).

The elastomer volume fraction v_{Rf} is then calculated from the Ellis and Welding equation (Swapna et al., 2016) (Equation (3)). The carbon black content was neglected in the calculation of the cross-link density as it is the same for all materials tested.

$$v_{Rf} = \frac{\frac{(m_d - m_f)}{\varrho_c}}{\frac{(m_d - m_f)}{\varrho_c} + \frac{m_s - m_d}{\varrho_s}} \quad \text{Equation 3}$$

Where:

m_d is the weight of the de-swollen sample;

m_s is the weight of the swollen sample;

m_f is the weight of filler;

ϱ_c is the density of standard NBR compound equal to 1,22 g/cm^3;

ϱ_s is the density of the toluene equal to 0,866 g/cm^3.

The degree of devulcanization (decrease in the crosslink density) D (%) was calculated with Equation 4

$$D = 1 - \frac{\nu_f}{\nu_i} \quad \text{Equation 4}$$

Where ν_f is the crosslink density of the devulcanized sample and ν_i is the crosslink density of industrial NBR scrap.

The hardness of the compounds was measured in Shore A hardness for 3 s following ISO 48–4 (ISO 48-4, 2018), using an automatic Shore PC type A hardness tester.

Mechanical tensile tests were conducted at cross-head rate of 100 mm/min to ISO 37:2017 type 2 (ISO 37, 2017). Each compound was measured three times.

The morphology and slag particles distribution in the NBR compounds were evaluated through scanning electron microscopy (SEM) observations of the surface fracture of specimens broken during the tensile test, after coating the surface with sputtered gold.

Dynamic mechanical analysis was performed in tensile mode at a frequency of 1 Hz and room temperature. The imposed strain was varied between 0,005% and 50% to observe the storage modulus at low and high plateaus. The analysis was conducted on nominal 1 × 5x30 mm specimens, with two repetitions.

The dependencies of E′ and E″ on the strain amplitude have been modeled by Kraus (Heinrich and Klüppel, 2002) and successively modified by Ulmer (1996) according to Equation (5) and Equation (6).

$$E'(\gamma) = E_\infty + \frac{E'_0 - E'_\infty}{1 + (\varepsilon'_c)^{2m'}} \quad \text{Equation 5}$$

$$E''(\gamma) = E''_\infty + \frac{2(E''_{max} - E''_\infty)(\varepsilon''_c)^{m'}}{1 + (\varepsilon''_c)^{2m'}} + (E''_{max} - E''_\infty)\, e^{\left(-\frac{\varepsilon}{\varepsilon_2}\right)} \quad \text{Equation 6}$$

Where ε'_c represents the strain amplitude corresponding to 2/3 $(E'_0 - E'_\infty)$ and ε''_c denotes the strain at which the E″ reaches its maximum E''_{max}. E'_0 is the storage modulus at low strain (<0,01%); E'_∞ and E''_∞ are the asymptotic plateau values of both moduli at high strain amplitudes, respectively; ε_2 and m' and m'' are non-negative phenomenological exponents used to fit the experimental data (Lion et al., 2003; Kim et al., 2020). These latter parameters were determined using the Excel solver function to find the best fit of the experimental data.

Recovery tests of the low strain amplitude dynamic modulus were also performed following the application of high amplitude dynamic strain. A recovery time of 5 min was used with the same test fixture.

3. Results and discussion

3.1. slag characterization

The grain size distribution of the EAF slag was determined through sieving analysis using stacked sieves with progressively smaller mesh sizes, ranging from 500 μm down to 50 μm. The granulation method employed reduces the particle size of the slag, resulting in almost 40% of it being below 100 μm. This particle size is acceptable for use as a filler and is roughly equally divided into the 0–50 μm and 50–100 μm ranges. The most populated particle size range is between 150 and 300 μm, with over 80% of the particles being smaller than 300 μm.

Concerning the EAF slag's microstructure and chemical composition, the existing literature establishes that they are influenced by two key factors: the specific cooling techniques applied during slag removal and the composition of the ferrous scrap materials undergoing smelting (Tossavainen et al., 2007; Engström et al., 2010; Mombelli et al., 2019). Consequently, the relationship between the slag's mineralogical phases and chemical composition significantly impacts the leaching behavior, which in turn affects its environmental impact. Therefore, it is important to establish correlations between the characteristics of the slag, such as its chemical composition and the phases present, and its tendency to leach heavy metals. The chemical composition of the EAF slag determined by XRF is reported in Table 2 and it falls within the conventional chemical composition of slag from carbon steel, with a FeO content of 35,5%, CaO 29%, SiO2 13,8%, and other oxides in smaller quantities. Table 2 also reports the binary basicity index BI2, expressed as the ratio of CaO/SiO_2. However, the quaternary basicity index BI4, formulated as $(CaO + MgO)/(SiO_2+Al_2O_3)$, is considered a more comprehensive indicator, accounting for the influence of Al_2O_3 and MgO on chromium leaching behavior in Cr-spinels, particularly in slags with a low presence of these spinel stabilizers oxides (Mombelli et al., 2016a, 2016b, 2018). Literature studies (Mombelli et al., 2018; Cabrera-Real et al., 2012; Arredondo-Torres et al., 2006) have associated the coexistence of Ca-chromate ($CaCrO_4$) and Cr-spinel with an IB4 range of 2–3, similar to the present research. These findings indicate that the leachability of chromium, as observed in the leaching test (Fig. 4), may be linked to the existence of an unstable spinel phase and calcium-ferrite, identified as brownmillerite through SEM-EDS analysis (Fig. 2). Moreover, a reduced presence of spinel-forming species like MgO and Al2O3 can facilitate the leaching of vanadium (V) (Mombelli et al., 2016a).

Considering this, the leaching of certain elements was found to be correlated with the presence and amount of certain oxides. In particular, the levels of CaO, SiO_2, Al_2O_3, and MgO influence the leaching behavior of V and Cr (Mombelli et al., 2016a).

In the case of slag with low Al_2O_3 (less than 3% wt) in the brownmillerite phase ($Ca_2(Al,Fe)_2O_5$), aluminum can be replaced by vanadium and/or chromium oxides. As brownmillerite is a hydraulic phase, hydration leads to the release of Cr and V (Mombelli et al., 2016a).

Cr leachability, empirical evidence indicates an association with non-stable spinel formation, a relationship predominantly affected by the cooling rate rather than the chromium oxide content. As elucidated by Roberti et al. (Gelfi and Cornacchia, 2010) the cooling rate exerts a pronounced influence on Cr leaching dynamics, inducing modifications in slag phases and their solubility, independent of the initial Cr_2O_3 concentration.

Fig. 2 illustrates the SEM-EDXS analysis of an EAF slag specimen, which has been polished metallographically and examined using the

Table 2
EAF slag chemical composition [%wt]and basicity indexes.

SiO_2	Al_2O_3	Fe_2O_3	MnO	CaO	MgO	P_2O_5	TiO_2	Cr_2O_3	S	Na_2O	K_2O	F
13,8	2,5	35,5	6,2	29,0	9,6	0,5	0,4	2,0	0,0	0,5	0,0	0,1

CaO/Al_2O_3 [-]	Al_2O_3/SiO_2 [-]	IB2 CaO/SiO_2 [-]	IB4 $(CaO + MgO)/(SiO_2+Al_2O_3)$ [-]
11,7	0,2	2,1	2,4

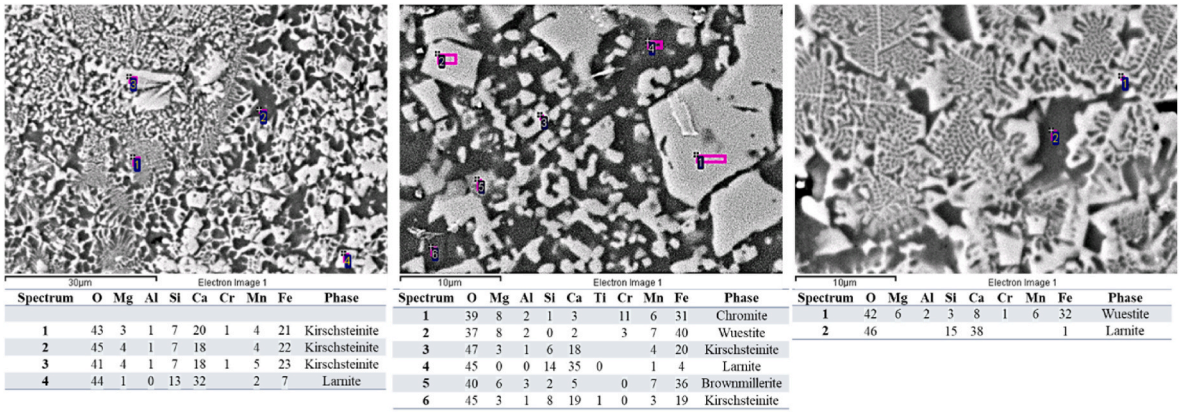

Spectrum	O	Mg	Al	Si	Ca	Cr	Mn	Fe	Phase
1	43	3	1	7	20	1	4	21	Kirschsteinite
2	45	4	1	7	18		4	22	Kirschsteinite
3	41	4	1	7	18	1	5	23	Kirschsteinite
4	44	1	0	13	32		2	7	Larnite

Spectrum	O	Mg	Al	Si	Ca	Ti	Cr	Mn	Fe	Phase
1	39	8	2	1	3		11	6	31	Chromite
2	37	8	2	0	2		3	7	40	Wuestite
3	47	3	1	6	18			4	20	Kirschsteinite
4	45	0	0	14	35	0		1	4	Larnite
5	40	6	3	2	5		0	7	36	Brownmillerite
6	45	3	1	8	19	1	0	3	19	Kirschsteinite

Spectrum	O	Mg	Al	Si	Ca	Cr	Mn	Fe	Phase
1	42	6	2	3	8	1	6	32	Wuestite
2	46			15	38			1	Larnite

Fig. 2. SEM back-scattered electron (BSE) image of slag microstructure [% wt] with its EDXS analysis on metallographically polished sample.

back-scattered electron (BSE) mode.

The phase morphology showcases the influence of swift cooling, evident in the development of an extremely fine dendritic structure and somewhat larger angular phases. The occurrence of these fine phases indicates that the slag was subjected to rapid cooling, a method generally employed to foster the creation of a vitreous phase, thereby reducing the leaching of heavy metals. SEM-EDXS analysis dentified different mineralogical phases. The darker phase, characterized by a high content of Ca and Si, has been identified as larnite (Ca_2SiO_4). Additionally, other silicates such as kirschsteinite ($CaFe^{2+}SiO_4$) and brownmillerite ($Ca_2(Al,Fe)_2O_5$) have been also identified. The lighter phase, rich in Fe, has been identified as wuestite (FeO), detected both in relatively coarse areas and at the edges of very fine dendritic structures. Finally, a spinel phase, identified as ferrocromite (Fe-Cr_3O_4), was observed with its characteristic angular shape. This phase is considered to be responsible for chromium leaching, due to its unstable form (Mombelli et al., 2018). Larnite, as documented in several scientific sources (Gobetti et al., 2023c; Gelfi and Cornacchia, 2010; Adib et al., 2015), exhibits a remarkable susceptibility to dissolution upon exposure to water due to hydration processes. This dissolution mechanism plays a pivotal role in modulating the Ca concentration within the leachate, thereby significantly influencing the ultimate pH of the surrounding environment (Mombelli et al., 2016b). According to the literature (Geiβler et al., 2015), a discernible correspondence between the leaching behavior of V and Ca has been determined. Particularly, an escalation in the Ca leaching corresponds to a notable reduction in the V concentration detected in the eluate.

Brownmillerite, as described in numerous scientific studies (Mombelli et al., 2016b; Gelfi and Cornacchia, 2010; Strandkvist et al., 2020), appears to be the predominant phase correlated to Cr leaching. While its stoichiometric formula does not explicitly contain chromium, scientific investigations suggest the plausibility of chromium substituting for other elements or contributing as an interstitial inclusion, thereby favoring the formation of potentially unstable phases.

Spinel structures play a crucial role in immobilizing Cr and preventing its leaching into the environment. However, unstable spinels can lead to Cr leaching from the slag if the spinel-forming species are not properly combined. The presence of high levels of spinel-forming species such as MgO and Al_2O_3, along with a low presence of CaO and SiO_2, is essential for stable spinel formation and for preventing Cr leaching (Mombelli et al., 2016c).

Concerning wuestite, its dissolution kinetics appear to be closely related to the FeO/MgO ratio (Strandkvist et al., 2020). Remarkable observations indicate suppression of Cr leaching when FeO content exceeds 70 wt%, with dissolution levels remaining below 60 wt%. Furthermore, the findings of Mombelli et al. (2018) suggest that the presence of Cr in magnesio-wüstite appears to be decoupled from its leaching dynamics and instead shows a tendency to mitigate the overall leaching of Cr.

The leaching test was performed on EAF slag with different grain sizes, all below 4 mm, according with the CEN EN 12457-2 standard (UNI, 2004). Furthermore, tests were performed on various fine grain size ranges: 0–50 µm, 50–100 µm, 100–150 µm, and 150–300 µm. The results of the leaching tests are shown in Fig. 3. It can be observed that, generally, smaller slag grain sizes lead to higher leaching levels of Mo and Cr, as well as increased electrical conductivity of the eluate. In contrast, the leaching values for pH and V are not significantly influenced by the grain size, which aligns with previous research findings (David et al., 2017).

Notably, Cr leaching remains minimal (below 0.05 mg/l) for slag grains smaller than 4 mm, but increases to about 0.2 mg/l for grain sizes in the 50–100 µm, 100–150 µm, and 150–300 µm ranges, and further rises to 0.35 mg/l for the 0–50 µm range. This increase in Cr leaching is likely due to the presence of unstable spinel phases, which enhance the contact surface area with water as the grain size diminishes.

3.2. Compound characterization

3.2.1. Crosslink density

The crosslink density of standard NBR, 100% recycled NBR, and 100% recycled NBR filled with 10% [v/v] EAF slag of grain sizes 0–50 µm and 50–100 µm was determined using the Flory-Rehner equation (Flory et al., 1943; Mok and Eng, 2018). The study aimed to evaluate the influence of the recycling process through calendering (indicated by the hatched area) and subsequent compression molding (indicated by the solid area).

The results indicate that the crosslink density of recycled NBR decreases after the calendering process, with a more pronounced reduction

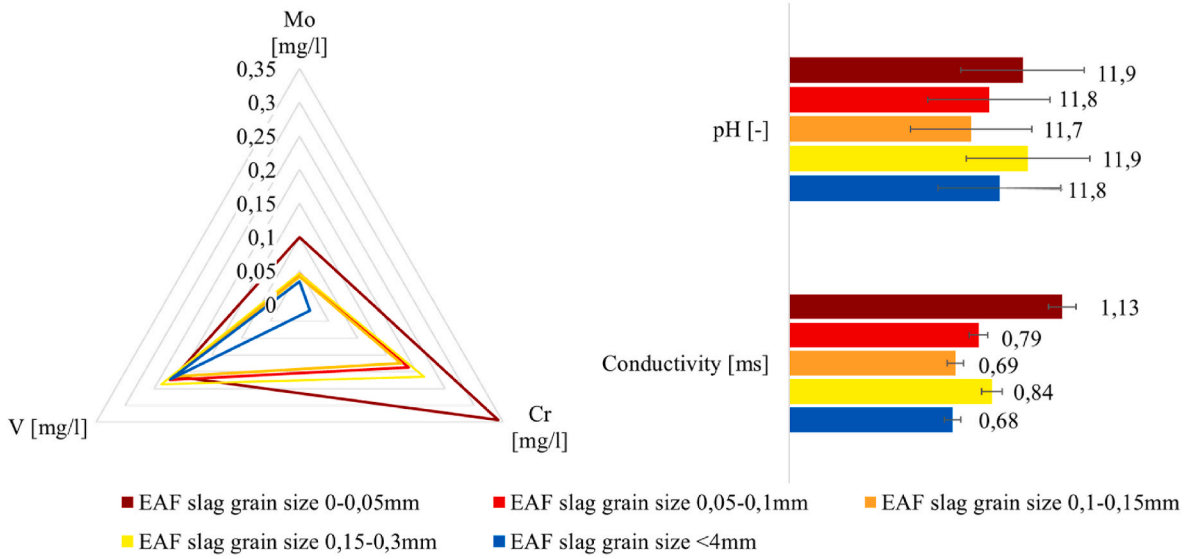

Fig. 3. Leaching test results of EAF slag in different granulometry. The maximum detected leaching value for each material is reported.

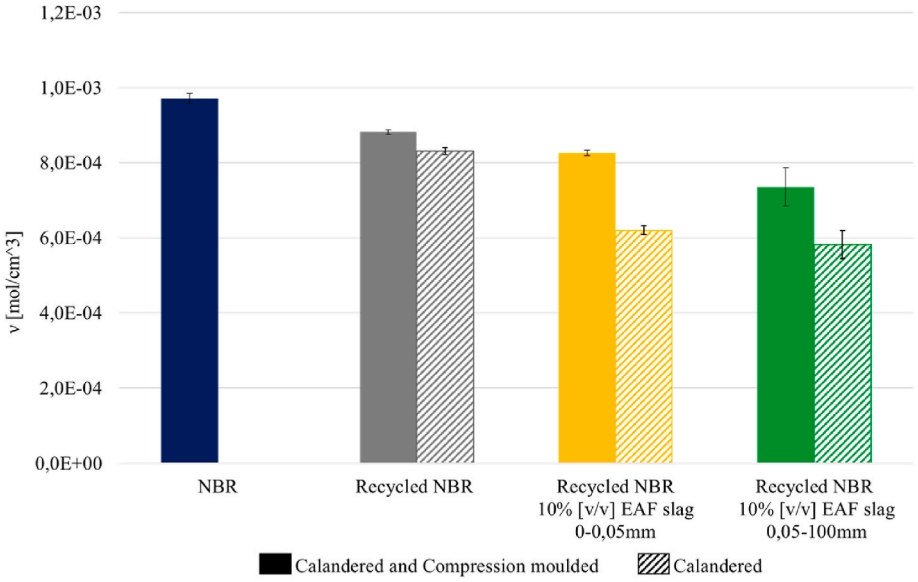

Fig. 4. Crosslink density determined by Flory-Rehner equation.

observed in the presence of slag particles in both studied grain size ranges. This reduction is likely due to the rigid particles limiting the available space for the polymer matrix to extend during the calendering process. This constraint increases the stress on the macromolecular network, leading to more significant alterations. As anticipated, compression molding leads to an increase in the crosslink density for each material, with the final crosslink density comparable to that of virgin NBR. It is worthwhile to notice that the recycled NBR filled with slag in 0–50 μm grain size range exhibits a slightly higher crosslink density slightly than that filled with slag in the 50–100 μm grain size range at equal volume fraction.

The crosslink density in filled rubber can act as a measure of the interaction between rubber and filler, as evidenced by the rise in the bound rubber fraction (Thomas et al., 2017). The filler particles are encased by a fixed NBR layer formed through interaction with slag (Gobetti et al., 2023b). The slag particles might be encased in a rubber layer with a high modulus, and then overlaid with a clay layer having a low modulus. This resulting rigid amorphous phase enhances the NBR composite's elevated crosslink density and tensile modulus (Thomas et al., 2017). As the tested composites vary not in the quantity of filler but in the size of filler grains, finer-grained filler will inherently offer a larger surface area for rubber adhesion. Therefore, these findings suggest a noticeable interaction between slag and NBR.

The percentage of devulcanization in reclaimed rubber serves as a valuable metric for evaluating the effectiveness of the recycling process. Generally, a higher devulcanization percentage reflects a more efficient recycling process. Experimental results presented in Table 3 demonstrate that the devulcanization percentage of recycled NBR filled with EAF slag (in both grain sizes) exceeds that of the recycled NBR without filler. This indicates that the addition of EAF slag as a filler in the recycled NBR enhances the devulcanization process, thereby improving the efficiency of rubber recycling. Specifically, at equivalent filler volume fractions, recycled NBR filled with EAF slag in the 50–100 μm grain size range exhibits a slightly higher devulcanization percentage compared to that filled with EAF slag in 0–50 μm grain size range. These findings suggest that the particle size of the EAF slag filler can influence

Table 3
Devulcanization degree of recycled NBR compounds by calendering and subsequent compression molding.

Material	Devulcanization [%]	
	Calendered	Calendered and compression molded
Recycled NBR	14% ± 0,6%	9% ± 1,5%
Recycled NBR 10% [v/v] EAF slag 0-0,05 mm	36% ± 1,0%	15% ± 0,9%
Recycled NBR 10% [v/v] EAF slag 0,05–0,1 mm	40% ± 1,2%	24% ± 0,8%

the devulcanization percentage of recycled NBR. Furthermore, the subsequent compression molding of recycled rubber via calendering induces new vulcanization even in the absence of additional crosslinking agents.

3.2.2. Hardness

The results of the hardness test are depicted in Fig. 5. The hardness value of recycled NBR falls within the tolerance range of 60 ± 5 mIRHD, while the incorporation of rigid particles enhances the hardness of the composite. Specifically, at equal filler content, the grain size influences the results of hardness test. Recycled NBR filled with slag particles ranging from 0 to 50 μm exhibits a hardness value of about 72 mIRHD, whereas the same amount of slag with grain size 50–100 μm yields a hardness value of 67mIRHD. This slight difference can be attributed to variations in filler surface areas, affecting the adhesion of rubber and resulting in a higher constrained polymer fraction. This test further suggests a favorable interaction between NBR and EAF slag.

3.2.3. Tensile properties

The tensile stress-strain curves depicting virgin NBR, recycled NBR, and slag-filled recycled NBR are shown in Fig. 6a.

The mechanical recycling process exerts the most significant influence on the tensile properties. This process inevitably disrupts the macromolecular structure of polymeric materials, including thermoplastics (Gobetti and Ramorino, 2020). In vulcanized rubbers, it not only severs the crosslinks but also damages the main chains. However, through the recycling steps of calendering and compression molding, the material achieves homogeneity and workability, enabling it to be molded into new shapes. Despite the resulting shapes being of relatively simple geometry, this process can yield significant environmental and economic benefits for the industry. Notably, while the most affected property experiences a moderate decrease, with the stress at break reducing from an average of 16 MPa–11 MPa, the strain at break undergoes a more substantial reduction of approximately 40%, attributed to the decrease in macromolecular weight.

Regarding its role as a filler, slag behaves comparably to traditional non-reinforcing fillers like calcium carbonate (Gobetti et al., 2024b). These fillers are commonly added to enhance material stiffness and reduce overall costs. This study suggests that slag can serve as a viable alternative to these conventional fillers. Specifically, the material filled with EAF slag in finer granulometry (0–50 μm) exhibits a more pronounced reduction in strain at break. This may be attributable to increased material stiffness, as evidenced by the elastic modulus. However, existing literature suggests that as filler grain size decreases, stress and strain at break typically improve (Kudori and Ismail, 2020; Khongwong et al., 2019). This phenomenon is not observed in the current study. The deviation from expected trends can be attributed to differences in filler geometry across various to grain size ranges, as illustrated in Fig. 7.

As regards the elastic modulus both, that defined as the slope of the first linear section of the stress-strain curve E and that defined as the slope of the secant at 100% strain, are shown in Fig. 6b, represented by the hatched and solid areas, respectively.

The investigation revealed that both moduli are enhanced by the inclusion of EAF slag as filler, with the recycled NBR filled with slag grains smaller than 50 μm demonstrating the highest moduli. This outcome corroborates the findings regarding hardness and crosslink density, which are associated with heightened interaction between the rubber and filler surfaces, thus validating the NBR-slag interaction.

Fig. 7 displays SEM micrograph and backscattering images of specimens' cross-sections post-tensile testing. The fracture surfaces reveal the quality of the recycling process, namely calendering and subsequent compression molding, resulting in a uniform NBR matrix comparable to that of a virgin NBR(Fig. 7a). In samples containing EAF slag, finer granulometry leads to excellent particle dispersion and improved adhesion with the matrix, evident from the minimal signs of particle extraction. A critical aspect highlighted by the tensile test results is the particle geometry. In the 50–100 range, numerous spherical particles are observed, enhancing mechanical properties by averting notch formation. Conversely, no spherical particles smaller than 50 μm were detected, with all particles in this range resulting from mechanical crushing, leading to the formation of angular particles that exacerbate notching. Hence, the optimal strategy to enhance tensile properties involves obtaining spherical particles as small as possible.

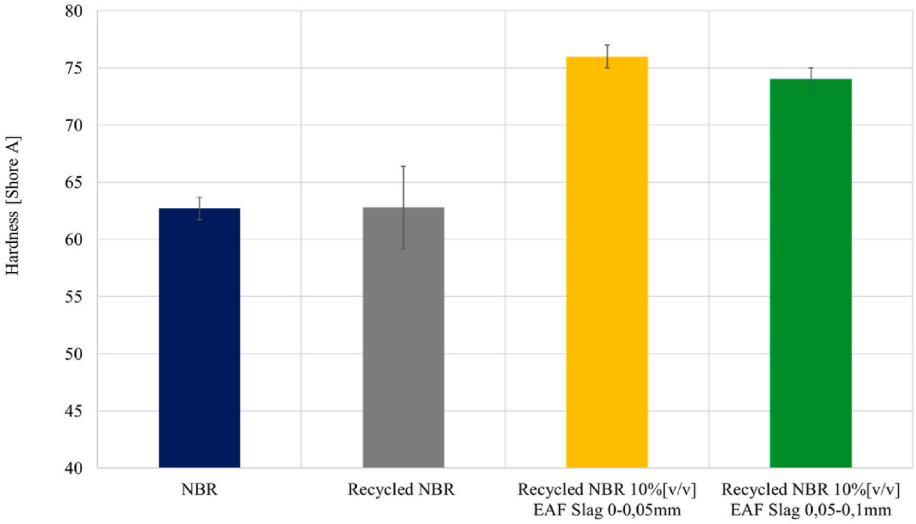

Fig. 5. Hardness values in mIRHD.

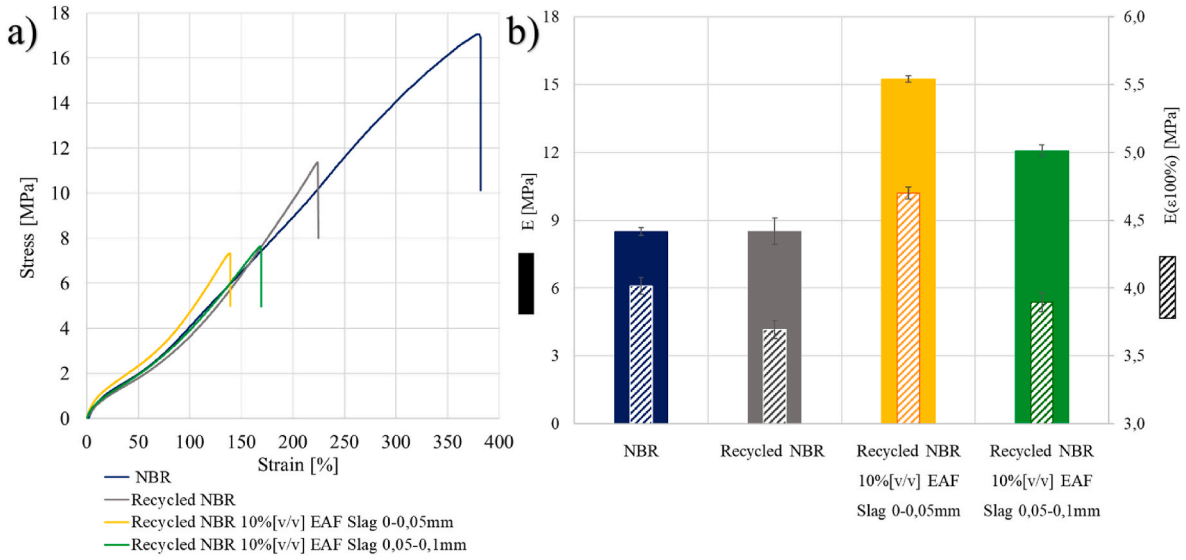

Fig. 6. Tensile stress optical strain mean curve for each material (100/mm/min, ISO 37 type 2).

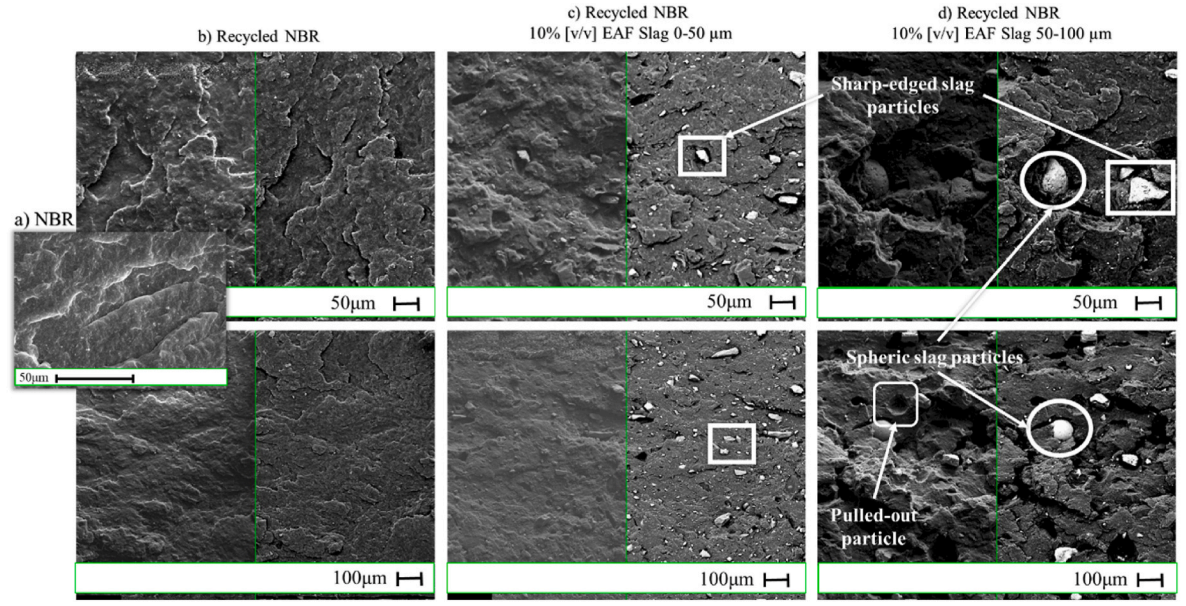

Fig. 7. SEM micrograph and backscattering images of cross sections of samples broken in tensile test. a) Virgin NBR; b) Recycled NBR; c) Recycled NBR filled with 10% [v/v] EAF Slag in grain size range 0–50 μm; d) Recycled NBR filled with 10% [v/v] EAF Slag in grain size range 50–100 μm.

3.2.4. Dynamic mechanical analysis

The dynamic behavior of rubber compounds is critical as it significantly influences the performance and functionality of rubber products. It is essential to understand the concepts of dynamic storage modulus (E′) and dynamic loss modulus (E″) when analyzing dynamic behavior., Vulcanized rubber compounds exhibit a non-linear response to applied strain amplitude, a phenomenon known as Payne effect. The Payne effect describes the behavior where E′ decreases, indicating a reduction in stiffness with increasing strain amplitude, while E' exhibits a peak.

In specific applications such as tires, belts, and anti-vibration devices, it is crucial to have high fatigue resistance. This requires maintaining low levels of energy dissipation to prevent excessive heat buildup, thereby necessitating a minimal Payne Effect in these scenarios. Conversely, in applications where fracture resistance is paramount, higher energy dissipation is beneficial as it helps divert energy away from a propagating crack, enhancing the elastomer's tear resistance. In these cases, a more pronounced Payne effect, allowing for greater energy dissipation, is advantageous. Since most engineering applications necessitate a balance between these conflicting requirements, it is essential to understand and model the Payne Effect (Rutherford et al., 2023).

Several theories have been proposed to explain the Payne effect, which can be broadly classified into two main categories: filler structure models and matrix-filler bonding and debonding models (Gauthier et al., 2004). However, two other factors, the hydrodynamic effect, and the rubber network, also influence the storage modulus, independently of the amplitude of the applied shear stress (Boonbumrung et al., 2016).

According to Payne (Payne, 1962; Shi et al., 2021), the variation in dynamic moduli under different strain amplitudes primarily results from the aggregation and dispersion dynamics within the filler network. In elastomers filled with carbon black, the structural rigidity depends largely on the strength of the bonds between the fillers. Another hypothesis suggests that the Payne effect arises from interaction between the matrix and filler materials (Gerspacher et al., 1996). This theory

centers on the concept of bound rubber, which exhibits reduced molecular mobility and effectively acts as additional crosslinks within the elastomer. As strain amplitude increases, a proposed mechanism involves the attachment and detachment of polymer chains at the filler interface.

Experimental findings across a strain amplitude range from 0.01% to 50% reveal a consistent storage modulus profile in all tested materials. This profile consists of a commencement with a low amplitude plateau, followed by a sharp decline, and concluding with a high amplitude plateau. It is noteworthy that the low amplitude storage modulus plateau is significantly elevated in filled NBR, particularly in samples containing 10% v/v EAF slag with grain sizes ranging from 0 to 50 μm, which exhibited the highest modulus. These observations align with the results obtained from hardness, crosslink density, and tensile tests, leading to similar conclusions. The study indicates that EAF slag-filled NBR displays a more pronounced Payne effect in comparison to recycled NBR without added slag, exhibiting dynamic behavior that is analogous to that of virgin NBR. A comparison between recycled NBR filled with 10% slag (grain size 0–50 μm) and 50–100 μm slag demonstrates a comparable fractional reduction in storage modulus, with both samples exhibiting approximately 90% reduction. This contrasts with the 85% reduction observed in recycled NBR without added slag.

The experimental results highlight that various types of fillers, beyond carbon black, influence the non-linear behavior of rubber compounds in response to strain amplitude, contributing to the Payne effect. This implies a close correlation between this phenomenon and the interaction between the filler and matrix, as the type and amount of carbon black remain constant across the tested compounds. At equivalent slag volume fractions, the compound containing smaller particles —thus offering a greater surface area for interaction— exhibits a higher storage modulus at low strain amplitudes, followed by a more pronounced decrease with increasing strain amplitude, eventually reaching a high storage modulus plateau, a consistent across all tested compounds.

It is noteworthy that as the slag-matrix interaction surface are increases, the deviation from linearity begins at lower strain amplitudes, as evidenced by the shift in the peak of E''_{max} at lower strain amplitudes. Lastly, it is observed that the behavior of 100% recycled NBR closely resembles that of virgin NBR, albeit a slightly higher loss modulus peak. This discrepancy could be attributed to the lower crosslink density in recycled NBR, resulting in a slightly higher viscous component. Of particular significance is the comparable behavior between recycled and virgin NBR under moderate deformations, suggesting the potential for recycled NBR to replace virgin materials in suitable applications. Moreover, the ability to adjust the dynamic properties by varying the slag particle size and loading fraction offers opportunities for tailoring these materials to meet specific requirements, thus contributing to sustainable material usage. The Kraus model, depicted by the solid lines in Fig. 8, accurately captures the experimental data for the storage modulus (E′) as illustrated in Fig. 8a. Regarding E'' (Fig. 8b) the Kraus prediction model, modified according to Ulmer (Ulmer, 1996; Heinrich and Klüppel, 2002), accurately aligns with the experimental data within the strain amplitude range of 0,05–10%.

Research was conducted to examine the partial restoration of the low amplitude storage modulus following the application of a substantial dynamic strain amplitude across all tested materials. Fig. 9 displays the results, illustrating the low amplitude storage modulus recorded after the imposition of the high strain amplitude plotted against time.

Following the reduction of E′ due to the application of a high-amplitude dynamic strain (50%), a low-amplitude dynamic strain (0.005%) is imposed and the speed of the material to recover its initial E′ is evaluated in percentage terms, where complete recovery corresponds to 100%.

It was observed that the incorporation of EAF slag facilitated the recovery process, although it reached a constant value that was lower than the initial measurement after a rapid recovery phase. It is noteworthy that materials filled with EAF slag exhibit a slightly higher and faster fractional recovery, particularly those containing slag grains

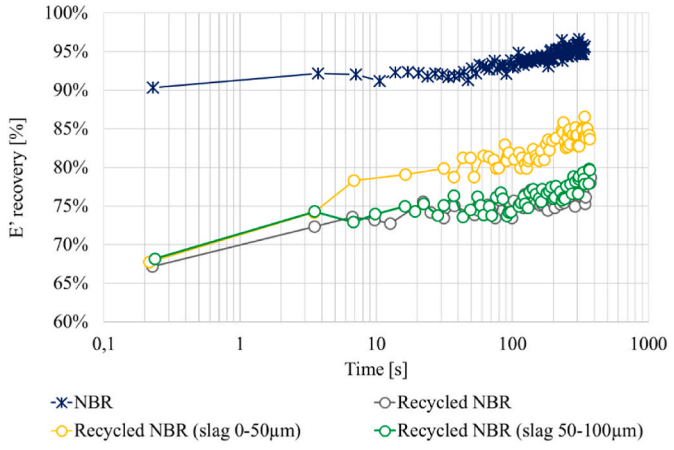

Fig. 9. Fractional recovery of low-strain storage modulus after high-amplitude dynamic strain.

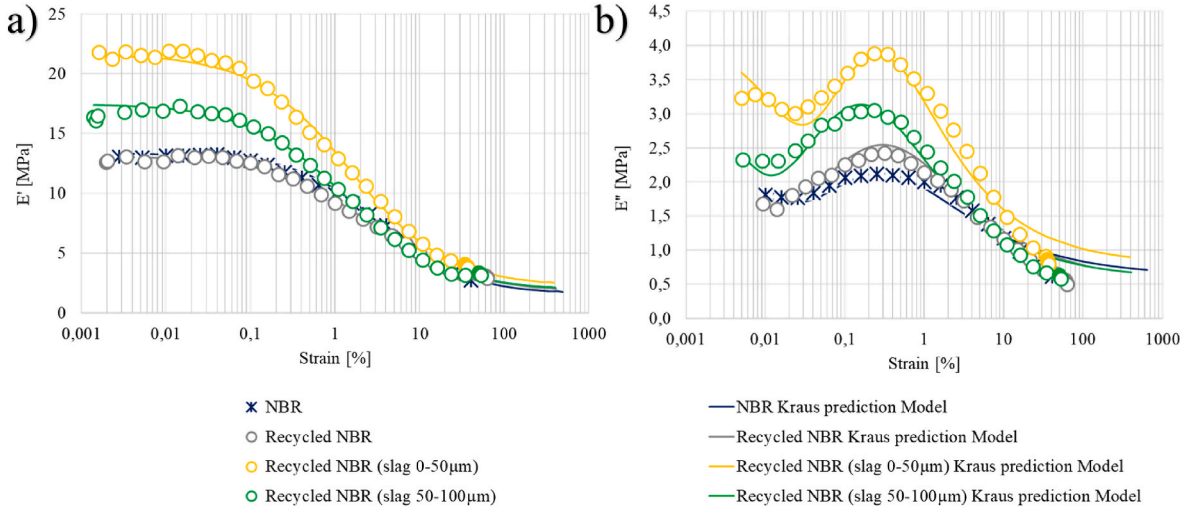

Fig. 8. a) Storage modulus (E′) and Kraus prediction model; b) Loss modulus (E″)) and Kraus prediction model.

smaller than 50 μm. This phenomenon indicates that the presence of a rigid amorphous rubber layer, constrained by rigid slag particles, facilitates elastic recovery following a significant strain amplitude disturbance. In contrast, recycled NBR displays significantly diminished fractional recovery in comparison to its virgin counterpart. This phenomenon aligns with its comparatively lower cross-link density, as evidenced by the inverse correlation between cross-link density and chain mobility. This latter phenomenon can be understood as the viscous sliding of macromolecules, resulting in a reduction in elastic recovery.

4. Conclusion

The present study delves into the valorization of two distinct industrial waste streams - nitrile butadiene rubber (NBR) scraps and electric arc furnace (EAF) slag - through the production of recycled NBR compounds filled with EAF slag particles. The findings underscore the potential of harnessing these waste materials, yielding both environmental and economic benefits.

A novel recycling process, conducted at room temperature without the addition of curative chemical agents or former rubber grinding, was employed for the recycling of NBR scraps. This mechanical recycling approach, relying solely on shear forces imparted during calendering, represents a significant departure from conventional thermal-mechanical or mechano-chemical recycling techniques. Notably, this method enables manufacturers to valorize their own scrap material without substantial capital investment, as it utilizes standard calenders commonly available in rubber processing facilities.

- The incorporation of EAF slag as a filler in recycled NBR compounds was found to enhance the devulcanization process, improving the efficiency of rubber recycling. The recycled NBR filled with EAF slag exhibited a higher degree of devulcanization compared to the unfilled recycled NBR, with the compound filled with slag in the grain size range of 50–100 μm displaying a slightly higher devulcanization percentage due to due to increased stretching exerted on the elastomeric matrix.
- The incorporation of rigid filler particles enhances the hardness of the composites. Specifically, when comparing composites with equal EAF slag content, the grain size of the filler affects the hardness. Recycled NBR filled with slag particles smaller than 50 μm exhibits slightly greater hardness compared to samples filled with an equivalent amount of slag with grain sizes ranging from 50 to 100 μm.
- The recycled NBR filled with EAF slag demonstrated a more pronounced Payne effect, characterized by a non-linear viscoelastic response, compared to the unfilled recycled NBR. This phenomenon is attributed to the interaction between the filler and the rubber matrix, suggesting that EAF slag, contributes to the non-linear behavior of rubber compounds. In particular, the rubber compound filled with slag in a grain size lower than 50 μm presents a more marked Payne effect probably due to a higher filler-matrix surface of interaction.
- The Kraus and Ulmer prediction model well describes the dynamic storage and loss modulus in strain amplitude sweep.
- It is noteworthy that the incorporation of EAF slag into recycled NBR compounds enabled a more expeditious fractional recovery of the low-strain amplitude storage modulus subsequent to the imposition of a high-amplitude dynamic strain. This effect is attributed to the presence of a rigid amorphous rubber layer constrained by the rigid slag particles, which enhances elastic recovery.

In conclusion, the findings of this study highlight the potential of reusing industrial wastes, such as EAF slag and rubber scraps, to produce functional rubber compounds with improved properties. The proposed recycling approach not only mitigates the environmental impact of these waste streams but also offers economic advantages by valorizing these materials as valuable resources in the context of industrial symbiosis. Potential applications for these recycled NBR/EAF slag compounds include automotive seals and gaskets, vibration isolation pads, and other simple geometry products benefiting from their tunable hardness, modulus, and energy dissipation capabilities.

CRediT authorship contribution statement

Anna Gobetti: Writing – original draft, Formal analysis. **Giovanna Cornacchia:** Writing – review & editing, Supervision. **Giorgio Ramorino:** Supervision.

Declaration of competing interest

The authors declare that they have no known competing financial interests or personal relationships that could have appeared to influence the work reported in this paper.

Acknowledgment

Authors thank Novotema S. p.A (Villongo (BG), Italy) for providing materials and test equipment for the characterization of EAF slag filled rubber composites.

Data availability

No data was used for the research described in the article.

References

Adhikari, J., Das, A., Sinha, T., et al., 2019. Grinding of Waste Rubber.
Adib, A., Domínguez, C., Rodríguez, J., et al., 2015. The effect of microstructure on the slow crack growth resistance in polyethylene resins. Polym. Eng. Sci. 55, 1018–1023. https://doi.org/10.1002/pen.23970.
Aliyah, F., Kambali, I., Setiawan, A.F., et al., 2023. Utilization of steel slag from industrial waste for ionizing radiation shielding concrete: a systematic review. Construct. Build. Mater. 382. https://doi.org/10.1016/j.conbuildmat.2023.131360.
Arredondo-Torres, V., Romero-Serrano, A., Zeifert, B., et al., 2006. Stabilization of MgCr2O4 spinel in slags of the SiO2-CaO-MgO-Cr2O3 system. Rev. Metal. (Madr.) 42, 417–424.
Barikani, M., Hepburn, C., 1992. Determination of crosslink density by swelling in the castable polyurethane elastomer based on 1/4 - cyclohexane diisocyanate and para-phenylene diisocyanate. Iran. J. Polym. Sci. Technol. 1, 1–5.
Bernal-Ortega, P., Anyszka, R., Morishita, Y., et al., 2023. Determination of the crosslink density of silica-filled styrene butadiene rubber compounds by different analytical methods. Polym. Bull. https://doi.org/10.1007/s00289-023-04749-x.
Boonbumrung, A., Sae-Oui, P., Sirisinha, C., 2016. Reinforcement of multiwalled carbon nanotube in nitrile rubber: in comparison with carbon black, conductive carbon black, and precipitated silica. J. Nanomater. 2016. https://doi.org/10.1155/2016/6391572.
Bristow, G.M., Watson, W.F., 1958a. Cohesive energy densities of polymers: Part 1. - cohesive energy densities of rubbers by swelling measurements. Trans. Faraday Soc. https://doi.org/10.1039/TF9585401731.
Bristow, G.M., Watson, W.F., 1958b. Cohesive energy densities of polymers: Part 2. - cohesive energy densities from viscosity measurements. Trans. Faraday Soc. https://doi.org/10.1039/TF9585401742.
Cabrera-Real, H., Romero-Serrano, A., Zeifert, B., et al., 2012. Effect of MgO and CaO/SiO on the immobilization of chromium in synthetic slags. J. Mater. Cycles Waste Manag. 14, 317–324. https://doi.org/10.1007/s10163-012-0072-y.
CEN EN 12457-2, 2002. Characterisation of waste - leaching - Compliance test for leaching of granular waste materials and sludges - Part 2: one stage batch test at a liquid to solid ratio of 10 l/kg for materials with particle size below 4 mm (without or with size reduction). Int. Stand.
Chittella, H., Yoon, L.W., Ramarad, S., Lai, Z.-W., 2021. Rubber waste management: a review on methods, mechanism, and prospects. Polym. Degrad. Stabil. 194, 109761. https://doi.org/10.1016/j.polymdegradstab.2021.109761.
David, Algermissen, Agnieszka, Morillon, Wendler, Barbara, et al., 2017. Control of Slag Quality for Utilisation in the Construction Industry (SLACON).
de Sousa, F.D.B., Zanchet, A., Marczynski, E.S., et al., 2020. Devulcanized EPDM without paraffinic oil in the production of blends as a potential application of the residues from automobile industry. J. Mater. Cycles Waste Manag. 22, 273–284. https://doi.org/10.1007/s10163-019-00938-x.
Dorigato, A., Rigotti, D., Fredi, G., 2023. Recent advances in the devulcanization technologies of industrially relevant sulfur-vulcanized elastomers. Adv Ind Eng Polym Res. https://doi.org/10.1016/j.aiepr.2022.11.003.
Engström, F., Adolfsson, D., Yang, Q., et al., 2010. Crystallization behaviour of some steelmaking slags. Steel Res. Int. 81, 362. https://doi.org/10.1002/srin.200900154, 31.

EUROFER The European Steel association, 2023. European Steel in Figures 2023.
European Commission, 2023. Commission Regulation (EU) 2023/2055 of 25 September 2023 Amending Annex XVII to Regulation (EC) No 1907/2006 of the European Parliament and of the Council Concerning the Registration, Evaluation, Authorisation and Restriction of Chemicals (REACH) as Rega.
Flory, P.J.P.J., Rehner, J., Rehner Jr., J., 1943. Statistical mechanics of cross-linked polymer networks II. Swelling. J. Chem. Phys. 11, 521–526. https://doi.org/10.1063/1.1723792.
Gao, J., Feng, Y., Feng, D., Zhang, X., 2021. Granulation performance by hybrid centrifugal-air blast technique for treatment of liquid slag. Powder Technol. 392, 204–211. https://doi.org/10.1016/j.powtec.2021.07.002.
Gauthier, C., Reynaud, E., Vassoille, R., Ladouce-Stelandre, L., 2004. Analysis of the non-linear viscoelastic behaviour of silica filled styrene butadiene rubber. Polymer (Korea). 45, 2761–2771. https://doi.org/10.1016/j.polymer.2003.12.081.
Geißler, G., Schüler, S., Raiger, T., et al., 2015. Factors of influence during and after the electric steel making process: characterization and optimization of electric arc furnace slag. In: Proceedings of the 8th European Slag Conference EUROSLAG. Linz (Austria).
Gelfi, M., Cornacchia, G.R.R., 2010. Investigations on leaching behavior of EAF steel slags. In: Electric Arc Furnace (EAF) Slag.
Gerspacher, M., O'Farrell, C.P., Yang, H.H., Tricot, C., 1996. Modeling of the carbon black reinforcement mechanism in elastomers. Rubber World 214, 27–49.
Gobetti, A., Ramorino, G., 2020. Application of short - term methods to estimate the environmental stress cracking resistance of recycled HDPE. J. Polym. Res. 27. https://doi.org/10.1007/s10965-020-02332-w.
Gobetti, A., Cornacchia, G., Ramorino, G., 2021a. Innovative reuse of electric arc furnace slag as filler for different polymer matrixes. Minerals 11, 832. https://doi.org/10.3390/min11080832.
Gobetti, A., Cornacchia, G., Ramorino, G., et al., 2021b. EAF slag as alternative filler for epoxy screeds , an example of green reuse. Sustain Mater Technol. 29, e00324. https://doi.org/10.1016/j.susmat.2021.e00324.
Gobetti, A., Cornacchia, G., Ramorino, G., 2022. Reuse of electric arc furnace slag as filler for nitrile butadiene rubber. J. Occup. Med. 74, 1329–1339. https://doi.org/10.1007/s11837-021-05135-6.
Gobetti, A., Cornacchia, G., Gelfi, M., Ramorino, G., 2023a. White steel slag from ladle furnace as calcium carbonate replacement for nitrile butadiene rubber : a possible industrial symbiosis. Results Eng. 18, 101229. https://doi.org/10.1016/j.rineng.2023.101229.
Gobetti, A., Cornacchia, G., La Monica, M., et al., 2023b. Assessment of the influence of electric arc furnace slag as a non-conventional filler for Nitrile Butadiene Rubber. Results Eng. 17, 100987. https://doi.org/10.1016/j.rineng.2023.100987.
Gobetti, A., Cornacchia, G., Petrogalli, C., et al., 2023c. Characterization of recycled end-of-life rubber tire filled with black slag. J. Reinforc. Plast. Compos. 0, 1–18. https://doi.org/10.1177/07316844231155398.
Gobetti, A., Marchesi, C., Depero, L.E., Ramorino, G., 2024a. Characterization of recycled nitrile butadiene rubber industrial scraps. J. Mater. Cycles Waste Manag. https://doi.org/10.1007/s10163-024-01932-8.
Gobetti, A., Tomasoni, G., Cornacchia, G., Ramorino, G., 2024b. Steel slag as a low-impact filler in rubber compounds for environmental sustainability. Mater. Manuf. Process. https://doi.org/10.1080/10426914.2024.2334696.
Gobetti, A., Cornacchia, G., Agnelli, S., et al., 2024c. A novel and sustainable rubber composite prepared from electric arc furnace slag as carbon black replacement. Carbon Resour Convers.
Grause, G., Buekens, A., Sakata, Y., et al., 2011. Feedstock recycling of waste polymeric material. J. Mater. Cycles Waste Manag. 13, 265–282. https://doi.org/10.1007/s10163-011-0031-z.
Heinrich, G., Klüppel, M., 2002. Recent advances in the theory of filler networking in elastomers. Adv. Polym. Sci. 160, 1–44. https://doi.org/10.1007/3-540-45362-8_1.
Hummen, T., Sudheshwar, A., 2023. Fitness of product and service design for closed-loop material recycling: a framework and indicator. Resour. Conserv. Recycl. 190. https://doi.org/10.1016/j.resconrec.2022.106661.
ISO 37, 2017. Rubber, Vulcanized or Thermoplastic — Determination of Tensile Stress-Strain Properties.
ISO 48-4, 2018. Rubber, Vulcanized or Thermoplastic — Determination of Hardness — Part 4: Indentation Hardness by Durometer Method (Shore Hardness).
Khongwong, W., Keawprak, N., Somwongsa, P., et al., 2019. Effect of Alternative Fillers on the Properties of Rubber Compounds.
Kim, D.Y.D.Y., Park, J.W.J.W., Lee, D.Y.D.Y., Seo, K.H.K.H., 2020. Correlation between the crosslink characteristics and mechanical properties of natural rubber compound via accelerators and reinforcement. Polymers 12, 1–14. https://doi.org/10.3390/polym12092020.
Kraus, G., 1984. Mechanical losses in carbon-black-filled rubbers. In: Applied Polymer Symposia, pp. 75–92.
Kudori, S.N.I., Ismail, H., 2020. The effects of filler contents and particle sizes on properties of green kenaf-filled natural rubber latex foam. Cell. Polym. 39, 57–68. https://doi.org/10.1177/0262489319890201.
Leblanc, J.L., 2002. Rubber-filler interactions and rheological properties in filled compounds. Prog. Polym. Sci. 27.
Leong, S.Y., Lee, S.Y., Koh, T.Y., Ang, D.T.C., 2023. 4R of rubber waste management: current and outlook. J. Mater. Cycles Waste Manag. 25, 37–51. https://doi.org/10.1007/s10163-022-01554-y.
Lion, A., Kardelky, C., Haupt, P., 2003. On the frequency and amplitude dependence of the Payne effect: theory and experiments. Rubber Chem. Technol. 76, 533–547. https://doi.org/10.5254/1.3547759.
Liu, H., Wang, X., Jia, D., 2020. Recycling of waste rubber powder by mechano-chemical modification. J. Clean. Prod. 245. https://doi.org/10.1016/j.jclepro.2019.118716.
Liu, S., Jing, Y., Tu, J., et al., 2022. Systematic investigation on the swelling behaviors of acrylonitrile-butadiene rubber via solubility parameter and Flory-Huggins interaction parameter. J. Appl. Polym. Sci. 139. https://doi.org/10.1002/app.52172.
Manso, J.M., Gonzalez, J.J., Polanco, J.A., 2004. Electric arc furnace slag in concrete. J. Mater. Civ. Eng. 16, 639. https://doi.org/10.1016/j.conbuildmat.2015.05.00.
Mok, K.L., Eng, A.H., 2018. Characterisation of crosslinks in vulcanised rubbers: from simple to advanced techniques. Malaysian. J. Chem. 20, 118–127.
Mombelli, D., Mapelli, C., Barella, S., et al., 2016a. The effect of chemical composition on the leaching behaviour of electric arc furnace (EAF) carbon steel slag during a standard leaching test. J. Environ. Chem. Eng. 4, 1050–1060. https://doi.org/10.1016/j.jece.2015.09.018.
Mombelli, D., Mapelli, C., Barella, S., et al., 2016b. The effect of microstructure on the leaching behaviour of electric arc furnace (EAF) carbon steel slag. Process Saf. Environ. Protect. 102, 810–821. https://doi.org/10.1016/j.psep.2016.05.027.
Mombelli, D., Mapelli, C., Di Cecca, C., et al., 2016c. Electric arc furnace slag: Study on leaching mechanisms and stabilization treatments | Scorie da forno elettrico ad arco: Studio sui meccanismi di rilascio e trattamenti di stabilizzazione. Metall. Ital. 108, 5–17.
Mombelli, D., Barella, S., Gruttadauria, A., et al., 2018. Effects of basicity and mesh on Cr leaching of EAF carbon steel slag. Appl. Sci. 9. https://doi.org/10.3390/app9010121.
Mombelli, D., Gruttadauria, A., Barella, S., Mapelli, C., 2019. The influence of slag tapping method on the efficiency of stabilization treatment of electric arc furnace carbon steel slag (EAF-C). Minerals 9, 706. https://doi.org/10.3390/min9110706.
Netinger Grubeša, I., Barišic, I., Fucic, A., et al., 2016. Characteristics and Uses of Steel Slag in Building Construction.
Payne, A.R., 1962. The dynamic properties of carbon black-loaded natural rubber vulcanizates. Part I. J. Appl. Polym. Sci. 6, 57–63. https://doi.org/10.1002/app.1962.070061906.
Pisciotta, M., 2020. The Volume Expansion of Artificial Road Aggregates Derived from Steelmaking Slags. Eur Transp - Trasp Eur.
Rooj, S., Basak, G.C., Maji, P.K., Bhowmick, A.K., 2011. New route for devulcanization of natural rubber and the properties of devulcanized rubber. J. Polym. Environ. 19. https://doi.org/10.1007/s10924-011-0293-5.
Rutherford, K.J., Akutagawa, K., Ramier, J.L., et al., 2023. The influence of carbon black colloidal properties on the parameters of the Kraus model. Polymers 15. https://doi.org/10.3390/polym15071675.
Sabzekar, M., Zohuri, G., Chenar, M.P., et al., 2016. A new approach for reclaiming of waste automotive EPDM rubber using waste oil. Polym. Degrad. Stabil. 129. https://doi.org/10.1016/j.polymdegradstab.2016.04.002.
Santos, E.M., Gomes, A.V., James, F., et al., 2020. Novel sustainable composites with geopolymeric steel slag and recycled from packing pet. In: Materials Science Forum.
Shi, X., Sun, S., Zhao, A., et al., 2021. Influence of carbon black on the Payne effect of filled natural rubber compounds. Compos. Sci. Technol. 203. https://doi.org/10.1016/j.compscitech.2020.108586.
Strandkvist, I., Pålsson, K., Andersson, A., et al., 2020. Minimizing chromium leaching from low-alloy electric arc furnace (EAF) slag by adjusting the basicity and cooling rate to control brownmillerite formation. Appl. Sci. 10. https://doi.org/10.3390/app10010035.
Swapna, V.P., Stephen, R., Greeshma, T., et al., 2016. Mechanical and swelling behavior of green nanocomposites of natural rubber latex and tubular shaped halloysite nano clay. Polym. Compos. 37, 602–611. https://doi.org/10.1002/pc.23217.
Teo, P.Ter, Anasyida, A.S., Nurulakmal, M.S., 2014. Characterization of ceramic tiles added with EAF slag waste. In: Advanced Materials Research.
The 15th global slag conference exhibition and awards global slag 2023 review. https://www.globalslag.com/conferences/global-slag/review/global-slag-review-2023, 2023–. (Accessed 8 April 2024).
Thomas, S., George, S.C., Thomas, S., 2017. Rigid amorphous phase: mechanical and transport properties of nitrile rubber/clay nanocomposites. Prog. Rubber Plast. Recycl. Technol. 33, 103–126. https://doi.org/10.1177/147776061703300204.
Tossavainen, M., Engstrom, F., Yang, Q., et al., 2007. Characteristics of steel slag under different cooling conditions. Waste Manag. 27, 1335–1344. https://doi.org/10.1016/j.wasman.2006.08.002.
Ulmer, J.D., 1996. Strain dependence of dynamic mechanical properties of carbon black filled rubber compounds. Rubber Chem. Technol. 69. https://doi.org/10.5254/1.3538354.
UNI, 2004. EN 12457-2 Characterisation of Waste - Leaching - Compliance Test for Leaching of Granular Waste Materials and Sludges - Part 2: One Stage Batch Test at a Liquid to Solid Ratio of 10 L/kg for Materials with Particle Size below 4 Mm (without or with size r.
Valentín, J.L., Carretero-González, J., Mora-Barrantes, I., et al., 2008. Uncertainties in the determination of cross-link density by equilibrium swelling experiments in natural rubber. Macromolecules 41. https://doi.org/10.1021/ma8005087.
Yehia, A., El-Sabbagh, S., 2007. Detection of crosslink density by different methods for natural rubber blended with SBR and NBR. Egypt. J. Solid. 30, 157–173.